

# Convergence-Guaranteed Time-Varying RRT Path Planning for Profiling Floats in 4-Dimensional Flow

Van T. Huynh<sup>a</sup>, Matthew Dunbabin<sup>a,b</sup>, and Ryan N. Smith<sup>c</sup>

<sup>a</sup>School of EECS, Queensland University of Technology, Brisbane, QLD, Australia

<sup>b</sup>Institute for Future Environments, Queensland University of Technology, Brisbane, QLD, Australia

<sup>c</sup>Department of Physics and Engineering, Fort Lewis College, Durango, CO, USA  
tv.huynh@qut.edu.au; m.dunbabin@qut.edu.au; rnsmith@fortlewis.edu

## Abstract

This paper presents a version of the Rapidly-exploring Random Tree (RRT) algorithm applied to autonomous, drifting underwater vehicles. The proposed extension is able to plan paths that guarantee convergence in the presence of time-varying ocean dynamics. The method utilizes 4-dimensional, ocean model prediction data as an evolving basis for expanding the tree from the start location to the goal. Results of the proposed method are validated through Monte-Carlo simulations. Results validate the importance of the temporal variance in path execution, and demonstrate the convergence guarantee of the proposed methods.

## 1 Introduction

Collection of long-term data is necessary to enhance our understanding of large-scale, dynamic ocean processes, as well as their complex spatio-temporal variability. Such long-term data gathering requires a persistent presence in the environment. One way to capture a time-series of spatio-temporally varying data is through the use of Autonomous Underwater Vehicles (AUVs) that are capable of long-period deployments (on the order of weeks to months), e.g., gliders [1, 2] and profiling floats [3]. These vehicles decrease actuation capability to save power for persistent navigation. However, with the compromise of actuation, it is challenging for these types of aquatic vehicles to reliably accomplish set-point trajectories due to extreme external disturbances, e.g., ocean currents. Therefore, it is imperative to address the problem of constructing a path planning strategy for such actuation-reduced aquatic vehicles that is able to predict and utilize these extreme disturbances.

Current work on path planning with uncertainties for persistent platforms is primarily focused on underwater gliders [4–8], there exists little research on path planning for profiling floats [9, 10]. Some recent works focused on multiple applications of profiling floats in physical oceanography and underwater imaging [11]. Nevertheless, the aforementioned research has motivated us to consider operation of profiling floats in highly-dynamic, coastal environments, or restrained areas like embayments. When operating in such environments, the vehicles are likely to be diverted away from the goal or the predetermined sensing location because they are constantly perturbed by external

forces; spatio-temporally varying currents that are the same order of magnitude as velocity of the vehicle.

To counteract the issue, this paper presents a convergence-guaranteed path planning method for persistent ocean monitoring that takes into account both disturbances of ocean currents and their time-dependency characteristic. Our approach is inspired by the ideas from Rapidly-exploring Random Tree (RRT) in the work of Hsu et al. [12] so that time-dependency and efficiency are considered. Due to vehicle’s operation in highly dynamic and disturbing environment, we includes a controllability verification step in our algorithm to ensure the convergence of the algorithm. We also provide analysis for convergence. To the best of the authors’ knowledge, this is the first paper dealing with the convergence-ensured, time-varying sampling-based algorithm under dynamic disturbances.

## 2 Background

Path planning for standard, actuated AUVs with propellers and control surfaces in the presence of water currents has been a centre of focus over the last decade. A number of approaches have been presented, such as Linear Optimization and Mixed Integer Linear Programming [13, 14], and A\* search [15]. However, these works consider vehicles operating mostly in a 2-dimensional (2D), horizontal plane.

Alvarez and Caiti [16] utilized numerical integration to predict rough paths for AUVs subject to ocean currents. Extending the work in [16], Alvarez et al. [17] developed a Genetic Algorithm (GA)-based path planning that takes into account the space-time structure of the ambient environment. In Alvarez et al. [17] the authors assume that the AUV travels at a constant speed with respect to the sea floor, i.e., the vehicle needs to vary its speed according to the current field so as to maintain its constant total velocity along the whole journey. In a similar scenario, Garau et al. [18] used the A\* algorithm to search for a minimum-time path that optimizes energy consumption. Garau et al. [19] continued to apply the algorithm in the previous work in the more realistic situation of current fields. However, as stated in those studies, the thrust power of the AUV is assumed constant throughout the operation. This kind of assumption is unjustified in reality. Furthermore, the aforementioned studies peculiarly concentrate on quasi steady-state ocean currents. They do not consider vehicle actuation limits and, especially, are unable to identify unfeasible tra-

jectories when the vehicles are operated in areas with strong ocean currents.

Addressing the problem of vehicle actuation limits, Kruger et al. [20] use a multi-dimensional cost function to generate minimum energy, time optimum, continuous paths in estuarine environments. Further extension of this work has been carried out by Witt and Dunbabin [21] to deal with the planning problem of generating time and energy optimum trajectories for actuated AUVs in dynamic ocean environments. This research has shown the potential to utilize tidal currents in such a way that vehicle range, endurance, and waypoint tracking are improved. Witt and Dunbabin also exposed the utilization of current variation along the vertical axis in path planning for AUVs. Considering the aforementioned works, and the references contained therein, there is little research on path planning algorithms examining both the controllability of the vehicles and the improvement of navigation.

Sampling-based path planning algorithms such as the probabilistic roadmap (PRM) [22] and Rapidly-exploring Random Trees (RRTs) [23] are being implemented heavily in recent years. These algorithms are well-known for their probabilistic completeness characteristic, i.e., rapidly exploring the space of interest and quickly returning a feasible solution if one exists. PRM\* and RRT\* are proposed to generate paths that are probably asymptotically optimal as the computation time increases [24]. Extensions of these sampling-based algorithms have also been developed to tackle uncertainty whilst maintaining asymptotic optimality [25]. These algorithms only concentrate on robots working without disturbances and do not approach dealing with extreme disturbances<sup>1</sup>, whose magnitude might be at the same order as that of the robot’s controls. As such, there will be no guarantee for convergence of the algorithms in such scenarios. Therefore, they cannot be applied directly to solve the motion planning problems under extreme conditions.

Attempting to apply sampling-based algorithms in extreme conditions, Rao and Williams [26] used RRTs for determining energy-optimal paths which account for ocean currents. A comparison of paths generated by the RRT and grid-based methods is presented demonstrating that RRTs offer an improvement in avoiding high-energy, shallow regions. However, [26] assumes that the ocean currents are time-invariant. Thus, this technique, to some extent, is unrealistic since ocean current magnitude and direction significantly vary temporally [27]. Motivated by the ideas from [12], we propose a novel algorithm that addresses extreme disturbances on underwater vehicles, and guarantees convergence to the end goal.

The proposed methodology is applied to the general case of path planning for profiling floats. This class of vehicle is considered the general case since profilers are minimally-actuated, as compared to standard AUVs with thrusters and control surfaces. Subsequently, if the algorithm is applicable to profilers, it will naturally extend to other AUVs having more control authority.

<sup>1</sup>Extreme disturbance is defined as external forces from ambient environment with the same order of magnitude as that of the internal control force

### 3 Equations of Motion

A profiling float is an underwater vehicle that freely drifts with the ambient currents, and can actively change its depth during a mission by adjusting its buoyancy. Intelligently controlling depth allows the profiler to choose appropriate ocean currents to carry the vehicle to a desired destination. An example profiling float is shown in Figure 1, with a detailed description found in [10].

Movement of the profiling float is determined primarily by ocean currents. The equations of motion of this vehicle involves both the ocean dynamics and the vehicle kinematics. Here, we present both the oceanic propulsion, referred to as Ocean Model Predictions (OMPs), and the kinematics of the float.



Figure 1: A profiling float prototype manufactured by Teledyne Webb Research, Inc.

#### 3.1 Ocean Model Prediction

The path planning method proposed in this paper is built upon the predictions a regional ocean model. The ocean model utilized is the regional ocean model system (ROMS). ROMS is split-explicit, free-surface, and topography-following-coordinate. Moreover, ROMS takes advantage of innovative algorithms to enhance the stability and robustness of the model, as well as its parallel efficiency. More detailed information on ROMS can be referenced in Shchepetkin and McWilliams [27, 28].

The ROMS data to be used in this paper is generated by the Jet Propulsion Laboratory (JPL), California Institute of Technology. ROMS ultimately provides hindcasts, nowcasts and hourly forecasts (up to 72 hours) for the SCB at various depths. Particularly, ROMS data divides non-uniformly the vertical direction into 24 discrete depths, ranging from 0 to 2000 m. Consequently, ROMS data is in four dimensions due to the fact that it gives predictions at different points of time and at various horizontal and vertical locations.

#### 3.2 Kinematics of Profiling fFloats

Provided that the vehicle is able to have neutral buoyancy at a predetermined depth, and that the centre of gravity (CG) and the centre of buoyancy (CB) are on the same vertical axis in the body-fixed coordinate frame  $\mathcal{B}$ , we define the vehicle’s state by the vector  $\boldsymbol{\eta} = (b_1, b_2, b_3)^T$ . The vector  $\boldsymbol{\eta}$  depicts the position of the vehicle relative to the inertial coordinate along longitude  $b_1$ , latitude  $b_2$ , and depths  $b_3$ .

Given that the ocean prediction data is presented in discrete-time format, and that the profiling float normally has unchanged control input over a single time epoch, we are motivated to consider the motion in discrete-time domain.

We can write the discrete-time equations of motions for profiling floats in Linear Time Varying state space form as follows,

$$\bar{\boldsymbol{\eta}}(k+1) = \mathbf{I}_2(k)\bar{\boldsymbol{\eta}}(k) + \mathbf{B}_{\bar{\boldsymbol{\eta}}}(k)\mathbf{u}(k) \quad (1)$$

$$\bar{\boldsymbol{\nu}}(k) = \mathbf{C}(k)\bar{\boldsymbol{\eta}}(k). \quad (2)$$

Here,  $\bar{\boldsymbol{\eta}}(k) = (b_1(k), b_2(k))^T \in \mathbb{R}^2$  is the state of the system representing its horizontal location at time epoch  $k$ .  $\bar{\boldsymbol{\nu}}$  stands for the system output.  $\mathbf{I}_2$  is the  $2 \times 2$  identity matrix. The output matrix  $\mathbf{C} = \mathbf{I}_2$ .

The control input is denoted by  $\mathbf{u}(k)$ . Here, the control input  $\mathbf{u}$  represents the depth selections of the vehicle to harness the appropriate ocean current.

Since the ROMS data contains 24 depth bins, we can denote  $\mathcal{U} = \{\mathbf{u}_1, \mathbf{u}_2, \dots, \mathbf{u}_{24}\}$  the set of control input vectors for the discrete-time system, where  $\mathbf{u}_j = (0, \dots, 0, 1, 0, \dots, 0)^T$  with unique nonzero entry  $j$ . By specifying  $\mathbf{u}$  in this form, the control input is bang-bang. Moreover, a control input of  $\mathbf{u}_1$  is interpreted as commanding the vehicle to the ocean surface, whereas a control input of  $\mathbf{u}_j, \forall j \in \{2, \dots, 24\}$ , is understood as commanding the profiling float to a specific depth corresponding to the ROMS output discretisation.

The input matrix  $\mathbf{B}_{\bar{\boldsymbol{\eta}}}(k)$  is a  $2 \times 24$  matrix giving the eastward and northward ocean velocities at each depth at location  $\bar{\boldsymbol{\eta}}$  from the ROMS model. So as to obtain  $\mathbf{B}_{\bar{\boldsymbol{\eta}}}(k)$ , we interpolate a set  $\mathbb{B}$  consisting of 4 similar matrices output from the ocean prediction model; one matrix for each discrete grid point of the ocean model prediction that defines the bounding box around the current position  $\bar{\boldsymbol{\eta}}$  of the vehicle. We can consider  $\mathbb{B}$  a lookup table for the predicted ocean currents at a given spatiotemporal location  $\bar{\boldsymbol{\eta}}(k)$ , and is interpolated from discrete nodes in the ocean prediction output. In this paper, we utilise a prediction model containing a total of 7826 grid points. Multiplication of  $\mathbf{u}$  and interpolated sets of currents  $\mathbf{B}_{\bar{\boldsymbol{\eta}}}(k)$  is ocean currents propulsion at time epoch  $k$  corresponding to location  $\bar{\boldsymbol{\eta}}$ .

## 4 Problem statement

The path planning problem for the profiler is to seek control inputs  $\mathbf{u} \in \mathcal{U}$  such that the vehicle moves from an initial configuration  $\boldsymbol{\eta}_0$  to a final configuration  $\boldsymbol{\eta}_f$  along locally absolutely continuous curve  $\gamma: I \mapsto Q$  when we apply such control input  $\mathbf{u}$ . The end conditions for  $\gamma$  is  $\gamma(0) = \boldsymbol{\eta}_0$  and  $\gamma(t_f) = \boldsymbol{\eta}_f$ . To steer the vehicle, we use only depths of the vehicle as direct control inputs. Therefore, the path planning problem is to find the set of depths  $\mathbf{u}(k)$  to achieve the final state  $\gamma(t_f)$  as close as possible to  $\boldsymbol{\eta}_f$  at time  $t_f$ .

The aforementioned depth choice is defined to be accomplished only when the vehicle successfully reach the goal destination. As we show in Section 5, a prerequisite for this condition to be satisfied is that a controllability check of control actions (ocean currents) in a specific region of ocean needs to be undertaken. If the controllability check for a region indicates that the region is able to direct the profiler in sufficient directions spanning the space, it is a fully-controllable region.

In brief, we need to address the problem of finding a path for the profiler subject to (1)-(2), travelling from an initial starting waypoint to a predetermined goal waypoint, and satisfying the following conditions,

- the planned path is placed inside a fully-controllable region,
- the planned path needs to be time-varying and takes into account dynamical disturbances from ocean currents of the ambient environment,
- convergence to the end goal is ensured although extreme disturbances exist.

## 5 Controllability Conditions

Given a profiling float and OMPs, are able to steer the vehicle to any destination within finite time. Here, we consider this by examining an accessibility set, the set of all admissible motion from each system state, as presented by the authors in [10]. The primary result from [10] is stated in Proposition 1.

**Proposition 1.** (*Conditions for controllability*) *The system given in Eq. (2) is controllable if and only if the convex hull of the accessibility set  $\mathcal{A}$  is compact and contains the origin.*

## 6 Time-invariant RRT Algorithm

---

**Algorithm 1:** The time-invariant RRT algorithm with incorporation of 4D OMP for AUV

---

**Input:** An initial waypoint  $\bar{\boldsymbol{\eta}}_0 = \{b_{10}, b_{20}\}$ , a target waypoint  $\bar{\boldsymbol{\eta}}_f = \{b_{1f}, b_{2f}\}$ , predicted ROMS data, a world space (the extracted region in ROMS)  $Q = \{NE_{corner}, SW_{corner}\}$ , and the termination ball  $\mathcal{B}_{\bar{\boldsymbol{\eta}}_f, r_f}$ .

**Output:** The switching sequence of depth control inputs.

```

1 world ← CreateWorld(NEcorner, SWcorner)
2 zstart ← GenerateNode( $\bar{\boldsymbol{\eta}}_0, 0, 0, 1$ )
3 zend ← GenerateNode( $\bar{\boldsymbol{\eta}}_f, 0, 1$ )
4 V ← {zstart} ; E ← ∅ ; G ← (V, E)
5 if || $\bar{\boldsymbol{\eta}}_0 - \bar{\boldsymbol{\eta}}_f$ || ≤ rf then
6   | path ← {zstart; zend}
7 else
8   | NumPaths ← 0
9   | while NumPaths < 1 do
10    | [G, flag] ← ExtendTree(G, zend, world)
11    | NumPaths ← NumPaths + flag
12 path ← FindMinimumPath(G, zstart, zend)
13 return Depths, path

```

---

Initially we consider a time-invariant RRT. We design this tree for incorporation of OMPs to plan a path for a profiling float through a quasi-steady ocean. The construction of time-invariant RRT incorporating 4D ROMS is presented in Algorithm 1. Moreover, Algorithm 1 is applied to underwater vehicles that are guided by changing vehicle depths during its course of action.

At the beginning, the algorithm creates a *world* space that is large enough to contain the initial and target waypoints. This world space specified by the South Western and North Eastern corners in Fig. 2 is situated in the region which is verified by the

controllability-check process to have varied directions of ocean currents.

The *GenerateNode* function in Algorithm 1 is used to create a tree node. Each RRT node is a structure whose two of its beginning fields contain the latitudinal and longitudinal coordinates. The third field is similar to a flag signalling the node in the tree that connects directly to the *EndNode*. The fourth field of the structure stores a cost associated with the node. Here we choose length of the path from *StartNode* as the cost. The next field of the RRT node is a back-tracking pointer pointing to the front node. And the final field is information about depth of the vehicle. This field contains a ROMS depth index corresponding to a specific depth that has an ocean current propulses the vehicle towards the *EndNode*.

Due to the fact that each tree node has six fields, the constructed RRT *tree* is in fact an array whose elements are six-field structures.

Before expanding the tree, the algorithm will check to see if the start node and end node are connectible by an ocean current propulsion. Particularly, if *StartNode* and *EndNode* falls within the ball  $\mathcal{B}_{\bar{\eta}_f, r_f}$  centred at the *EndNode* with radius  $r_f$ , the start node can connect directly to the end node without attempting to expand the tree.

If the start node is not connectible directly to the end node immediately, then the function *ExtendTree* will be activated to expand the tree. Figure 2 demonstrates the development of a time-invariant RRT tree when *ExtendTree* is called. Details of the *ExtendTree* function are presented in Algorithm 2. Because this is a time-invariant path planner, we assume that for this planner the ocean currents do not vary much over time, i.e., we only look at one hour of prediction of ROMS in the time-invariant algorithm.

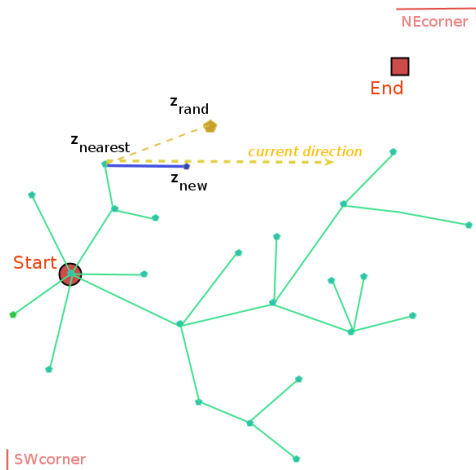


Figure 2: Illustration of tree expansion

For Algorithm 2 at a loop epoch, we note that the function *ExtendTree* randomly generates a point in the horizontal plane  $z_{rand}$ . It will then search all of the nodes in the tree for a node  $z_{nearest}$  that is nearest to the random node. Remember that right at such a nearest node, we have various oceanic layers containing ocean currents which flows along different directions. Such oceanic layers are also time-

dependent. If the assumption that ocean currents do not vary tremendously by time is upheld, Algorithm 2 will then choose a depth that yields a maximal ocean current from the nearest node  $z_{nearest}$  towards the random node  $z_{rand}$ . The process of depth selection is carried out by the function *FindSegmentLength*. The *FindSegmentLength* function also returns magnitude of the maximal ocean current and assigns it to *SegmentLength*. Based on direction of the selected ocean current  $(v_{cx}, v_{cy})$  at the chosen depth *NodeDepth*, we augment a new node  $z_{new}$  to the tree. Cost of the new node will be equal to summation of the cost of  $z_{nearest}$  and the magnitude of the selected ocean current (*SegmentLength*). Due to dynamics of the minimally-actuated underwater vehicles, their movement is bounded by the magnitude of propulsion of ocean currents. Consequently, instead of expanding the nearest node directly to the random node, the new node is just a *SegmentLength* away from the nearest node. After connecting the new node to the tree, back-tracking pointer of the new node points to  $z_{nearest}$  and the last field of the new node is assigned the ROMS index of the selected ocean depth *NodeDepth*.

When there is a node, which is named *next-to-end*, connectible to the end node, the algorithm will return a path originating from the start node to the the goal node. This path is chosen by considering costs of nodes right before the *next-to-end*, which we will call *next-to-last* nodes. Specifically, the algorithm will return the path containing the end node, the *next-to-end*, and a *next-to-last* node which has minimum cost among the *next-to-last* members. The *FindMinPath* utilizes backtracking pointers to pick out other nodes of the returned path.

The combination of Algorithms 1 and 2 differs from Rao's work [26] in its application domain. Our algorithm is used to guide the minimally-actuated vehicles whose control input is mainly depth-switching signals. The algorithm developed by Rao is applied for gliders. Unlike Rao's paper, we relax the assumption that distances between degrees of latitude and longitude are fixed. Moreover, in contrast to Rao's algorithm, we assume a larger column of water for the vehicle to utilize.

In addition, the time-invariant RRT we develop in this paper differs from the conventional RRT in the functions *ExtendTree*, *FindSegmentLength*, and *FindMinPath*. We can also see it requires the utilization of OMP data in the development of the tree. More importantly, the return structure from our proposed algorithm is a 2.5D RRT tree in the three-dimensional space. A visual representation is shown in Figure 3. The extra dimension in the tree represents the depth switchings for the vehicle.

There are some points that need to be clarified in the *ExtendTree* algorithm. First of all, when extending the nearest tree leaf towards the random node, it chooses a dive depth in ROMS with the largest current among the ocean currents at the nearest tree leaf location. Secondly, the tree will expand in whatsoever location of the random node, i.e., when the algorithm cannot pick a depth with current vector pointing in the Line of Sight (LoS) direction, it will still augment to the tree a node in the opposite of LoS under the

propulsion of minimum current at the tree leaf. This characteristic slightly differs the algorithm in this paper with effects of ocean currents from the conventional RRT that operates without effects from disturbances. The conventional RRT does not grow the tree against the random node; instead it extends the nearest tree leaf to the random node in any circumstances. For instance, consider the case depicted in Figure 4. Even though the nearest node forms a vector in the LoS direction with the random node, we still have the new node augmented to the side which is far away from the goal. This situation occurs when the algorithm is not able to pick a current close enough to the LoS. As a result, it will choose a minimal current in the out-of-LoS region. Furthermore, it should be noted that each node contains a cost which is the accumulation of magnitude of ocean current velocities. Finally, contrary to the conventional RRT, the path planning algorithm we propose guarantees convergence. Details of the convergence proof are presented in Section 7.1.

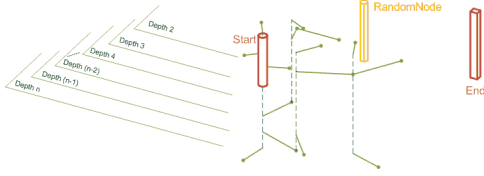


Figure 3: Illustration of 3D structure of the tree

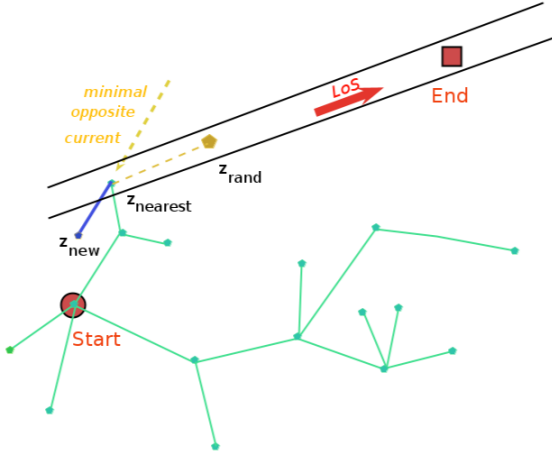


Figure 4: Expansion of the tree in the opposite LoS

Unlike the  $A^*$  approach in [26], we do not grid the whole space, but interpolate ROMS inside the horizontal space for the ocean currents at each node. The continuity of the space is preserved by taking this approach. Interpolating for the ocean current velocities also guarantees that our path planning algorithm aligns with real operation of underwater vehicles whose motion is not discrete but continuous.

We see that the resultant tree is 3D, accommodating both horizontal and vertical motions of the underwater vehicle. Additionally, it shows that at each node the vehicle is capable of switching to another depth before continue to move to the next node.

---

**Algorithm 2:** A tree extension algorithm for the time-invariant RRT

---

**Input:** The RRT tree  $G = (V, E)$ , the desired end node  $z_{end}$ , the world space ( $world$ ), and the ball  $\mathcal{B}_{\bar{\eta}_f, r_f}$ .

**Output:** An extended tree  $G' = (V', E')$ , a flag ( $flag$ ) signalling connectivity between the extended tree with the end node

```

1  $V' \leftarrow V; E' \leftarrow E$ 
2  $LoopFlag \leftarrow 0$ 
3 while  $LoopFlag == 0$  do
4    $z_{rand} \leftarrow RandomPointSeeding(world)$ 
5    $z_{nearest} \leftarrow Nearest(G, z_{rand})$ 
6    $[SegmentLength, NodeDepth, v_{cx}, v_{cy}] \leftarrow FindSegmentLenth(z_{nearest}, z_{rand})$ 
7    $cost \leftarrow InferNodeCost(z_{nearest}, SegmentLength)$ 
8    $z_{new} \leftarrow Steer(z_{nearest}, v_{cx}, v_{cy}, cost, NodeDepth)$ 
9    $V' \leftarrow V' \cup z_{new}; E' \leftarrow E' \cup \{(z_{nearest}, z_{new})\}; G' \leftarrow (V', E')$ 
10   $LoopFlag \leftarrow 1$ 
11 if  $\|z_{new} - z_{end}\| \leq r_f$  then
12    $flag \leftarrow 1$ 
13    $G' \leftarrow MarkConvergence(G')$ 
14 else
15    $flag \leftarrow 0$ 
16 return  $G', flag$ 

```

---



---

**Algorithm 3:** The time-varying RRT algorithm with incorporation of 4D OMP for AUV

---

**Input:** An initial waypoint  $\bar{\eta}_0 = \{b_{10}, b_{20}\}$ , a target waypoint  $\bar{\eta}_f = \{b_{1f}, b_{2f}\}$ , predicted ROMS data, a world space (the extracted region in ROMS)  $\mathcal{Q} = \{NE_{corner}, SW_{corner}\}$ , and the termination ball  $\mathcal{B}_{\bar{\eta}_f, r_f}$ .

**Output:** The switching sequence of depth control inputs.

```

1  $world \leftarrow CreateWorld(NE_{corner}, SW_{corner})$ 
2  $x_{start} \leftarrow GenerateTimeNode(\bar{\eta}_0, 0, 0, 1, 1, 1)$ 
3  $x_{end} \leftarrow GenerateTimeNode(\bar{\eta}_f, 0, 0, 1, branch_{end}, t_{end})$ 
4  $V \leftarrow \{x_{start}\}; E \leftarrow \emptyset; G \leftarrow (V, E)$ 
5 if  $ConnectionCheck(t \leftarrow 1, x_{start}, x_{end}, r_f)$  then
6    $path \leftarrow \{x_{start}, x_{end}\}$ 
7 else
8   forall the  $NumberOfTrees$  do
9      $NumPaths \leftarrow 0$ 
10    while  $NumPaths < 1$  do
11       $[G, flag] \leftarrow ExtendTVTree(G, x_{end}, world)$ 
12       $NumPaths \leftarrow NumPaths + flag$ 
13  $path \leftarrow FindMinimumPath(G, x_{start}, x_{end})$ 
14 return  $Depths, path$ 

```

---

## 7 Time-varying RRT Algorithm

So as to address the changes of the ambient propulsion forces, we propose a sampling-based path planning algorithm that takes into account the time-varying characteristics of the ocean.

A solution for a time-varying RRT utilising OMP is presented in Algorithm 3. Creation of the world space is the same as that in time-invariant RRT. However, we use the *GenerateTimeNode* function to generate a node for the time-dependent tree. Besides the six fields generated by *GenerateNode* in Algorithm 1, such function constructs a tree node with two more fields containing branch index and time, making each node a function of both time and 3D location. In other words, each node is mathematically represented as  $\mathbf{x}(t, x, y, z)$ . Because the starting node is also the tree root, we are able to specify both branch index and time for the starting node to be equal to one unit. Nevertheless, the branch index and time of the end node is unknown due to the time-dependent characteristics of the tree. Only when successfully expanding the tree to the goal node are we able to determine the goal node's tree branch and reaching time.

Unlike the time-invariant tree, the resultant tree grown by Algorithm 3 will be an array whose elements consists of up to eight fields.

---

**Algorithm 4:** The tree expansion algorithm for time-varying RRT

---

**Input:** The RRT tree  $G = (V, E)$ , the desired end node  $\mathbf{x}_{end}$ , the world space (*world*), and the ball  $\mathcal{B}_{\bar{\eta}_f, r_f}$ .  
**Output:** An extended tree  $G' = (V', E')$ , a flag (*flag*) signalling connectivity between the extended tree with the end node

```

1 while Tree is not extended do
2    $\mathbf{z}_{rand} \leftarrow \text{RandomPointSeeding}(\text{world})$ 
3    $[\mathbf{z}_{nearest}, t_{nearest}] \leftarrow \text{Nearest}(G, \mathbf{z}_{rand})$ 
4    $[\text{SegmentLength}, \text{NodeDepth}, v_{cx}, v_{cy}] \leftarrow$ 
5      $\text{FindTVSegmentLength}(\mathbf{z}_{nearest}, t_{nearest}, \mathbf{z}_{rand})$ 
6    $cost \leftarrow$ 
7      $\text{InferNodeCost}(\mathbf{z}_{nearest}, \text{SegmentLength})$ 
8    $\mathbf{z}_{new} \leftarrow$ 
9      $\text{Steer}(\mathbf{z}_{nearest}, v_{cx}, v_{cy}, cost, \text{NodeDepth})$ 
10   $t_{new} = t_{nearest} + 1$ 
11   $\mathbf{x}_{new} \leftarrow \{\mathbf{z}_{new}, t_{new}\}$ 
12   $V' \leftarrow V' \cup \mathbf{x}_{new}; E' \leftarrow$ 
13     $E' \cup \{(\mathbf{x}_{nearest}, \mathbf{x}_{new})\}; G' \leftarrow (V', E')$ 
14  if  $\|\mathbf{x}_{new} - \mathbf{x}_{end}\| \leq r_f$  then
15     $flag \leftarrow 1$ 
16     $G' \leftarrow \text{MarkConvergence}(G')$ 
17  else
18     $flag \leftarrow 0$ 
19  return  $G', flag$ 

```

---

For every evolution cycle of the RRT, *ExtendTVTree* first generates a random point  $\mathbf{z}_{rand}$ . The RRT will then search for a tree node  $\mathbf{x}_{nearest}$  that is nearest to  $\mathbf{z}_{rand}$ .  $\mathbf{x}_{nearest}$  has a node position  $\mathbf{z}_{nearest}$  at an epoch  $t_{nearest}$ . The RRT will then add a new node  $\mathbf{x}_{new}$  to the tree. The new node  $\mathbf{x}_{new}$  is associated with tree evolution at epoch  $(t + 1)$  and right

after the node  $\mathbf{x}_{nearest}$ . Likewise,  $\mathbf{x}_{new}$  has a node position  $\mathbf{z}_{new}$  and a time index  $t_{new} = t_{nearest} + 1$ .

A *FindTVSegmentLength* function determines the length between  $\mathbf{x}_{nearest}$  and  $\mathbf{x}_{new}$ . *FindTVSegmentLength* interpolates ROMS data at the location  $\mathbf{z}_{near}$  along both time and depth dimensions so as to return a maximum ocean currents originating from  $\mathbf{z}_{nearest}$  pointing towards  $\mathbf{z}_{rand}$ . We do not assume the vehicle moves along the direction between the nearest node to the random node with an amount equivalent to a projection of corresponding ocean currents onto the mentioned direction. Instead, we consider motion in the same directions as predicted ocean currents. To be more specific, in tandem with the time-invariant counterpart, *FindTVSegmentLength* does not necessarily choose an ocean current velocity vector aligning exactly with the straight line between  $\mathbf{z}_{rand}$  and  $\mathbf{z}_{nearest}$ . Should the LoS-directed ocean current not exist, it will pick a minimal ocean current against the LoS. We can state that the tree evolution abide the kinodynamics of both the profiling floats and the ocean.

With this approach, we are building more than a branch, e.g., assuming that there are  $l$  branches in total. At time 1 corresponding to the origin, RRT seeds a random point  $\mathbf{z}_{rand}$ . Since there is only one node at present, the RRT will then add a node  $\mathbf{x}_{newA1[2]}$  to the tree. Here,  $\mathbf{x}_{newAn[t]}$  represents an  $n^{th}$  new node augmented to the tree at time  $t$  and at location  $\mathbf{z}_{newAn}$ . Moreover, the subscript  $A$  indicates a branch index of the tree. In the second evolution cycle, the RRT will generate another random point  $\mathbf{z}_{rand}$ . The algorithm will then find either the origin or  $\mathbf{x}_{newA1[2]}$  is closer to  $\mathbf{z}_{rand}$ .

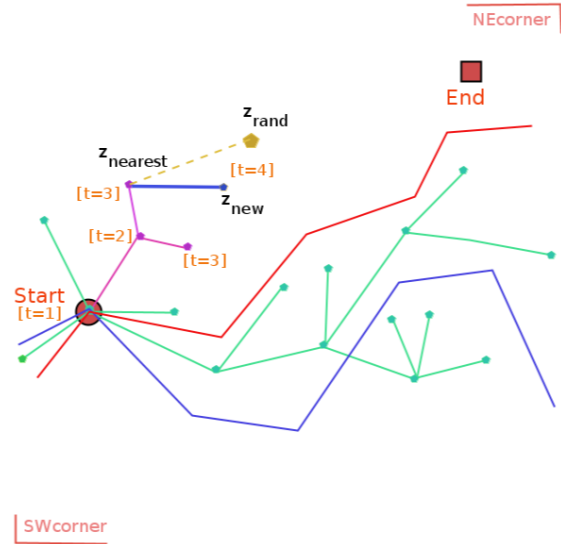


Figure 5: Illustration of time-varying expansion of the tree

Assume that the origin  $\mathbf{x}_{start[1]}$  is closer to  $\mathbf{z}_{rand}$ . RRT will augment a node  $\mathbf{x}_{newB1[2]}$  next to  $\mathbf{x}_{start[1]}$ . Consequently, there are two branches now. One of the branches evolves in the direction of  $\mathbf{x}_{newA1[2]}$ . The other one evolves in the direction of  $\mathbf{x}_{newB1[2]}$ . Both  $\mathbf{x}_{newA1[2]}$  and  $\mathbf{x}_{newB1[2]}$  are the planned position of the vehicle at time epoch 2.

If  $\mathbf{x}_{newA1[2]}$  is closer to  $\mathbf{z}_{rand}$ , the tree in direction  $\mathbf{x}_{newA1[2]}$  develops as normal, and a new node  $\mathbf{x}_{newA2[3]}$  is constructed.

In the third cycle, the tree will have three nodes. Let us find out how the tree grows when it has nodes  $\mathbf{x}_{start[1]}$ ,  $\mathbf{x}_{newA1[2]}$ , and  $\mathbf{x}_{newB1[2]}$ . After randomly seeding, another branch in the direction of  $\mathbf{x}_{newC1[2]}$  will appear if  $\mathbf{x}_{start[1]}$  is the only node closest to  $\mathbf{z}_{rand}$ . For the other cases, either  $\mathbf{x}_{newA1[2]}$  and  $\mathbf{x}_{newB1[2]}$  will be chosen. Without loss of generality, assuming that  $\mathbf{x}_{newA1[2]}$  is selected. A new node  $\mathbf{x}_{newA2[3]}$  is augmented to the branch  $A$  with a time index of 3 since its parent node is a node with time index 2. A visual illustration of time-varying expansion of the tree is depicted in Fig. 5, where different branches are represented by various colors.

In this approach, it is obvious that we differentiate the tree into subtrees, e.g.,  $A, B, C, \dots$ . Basically, whenever we add a new node into the tree, epoch associated with this new node will be one unit greater than the node right before this new node. Therefore, the tree index field specified in each node is assigned an increment number. The start node has a branch index of 1. Other nodes surrounding the origin node will get branch indices starting from 2.

It should be noted that our approach is not equivalent to construction of more than one RRT tree. In fact, we build branches with various time indices. So as to synthesize more-than-one trees, we can make change of *NumberOfTrees* in the Algorithm 3 to a value different from unity. If we have  $NumberOfTrees \geq 2$ , various paths with varied associated costs to the destination can be generated. The *FindMinimumPath* will extract a path with a minimum cost.

## 7.1 Analysis

We will prove convergence of the RRT algorithm for the profiler with incorporation of OMP. This proof is inspired by the works of Smith and Huynh [10] and Jouffroy et al. [9].

### Convergence of the time-varying algorithms

**Lemma 1.** *Given the controllability check showing that desired waypoints are in fully controllable of  $\chi_{free}$ , we can surely obtain planned paths to the goal region around  $\eta_f$ .*

*Proof.* In the deep-sea environments, there are several layers of currents. According to Jouffroy et al. [9], when there are more than or equal to three ocean currents whose directions spanning the horizontal space, we can guide the vehicle to the destination - actually around the destination.

Specifically, we often calculate

$$\theta = [\theta_1, \theta_2, \theta_3]^T, \quad (3)$$

where  $\theta_i, \forall i = 1, 2, 3$ , are the difference angle between the currents velocities  $(v_{c1}, v_{c2}, v_{c3})^T$  at each layer and the line of sight.

Consequently, if  $(v_{c1}, v_{c2}, v_{c3})^T$  spans the space, we can express any point in the horizontal space as a linear combination  $\sum_{i=1}^3 \alpha_i v_{ci}$ . So, by applying control  $u = \operatorname{argmin}(\theta)$ , we can always direct the profiler towards the region around the end node.  $\square$

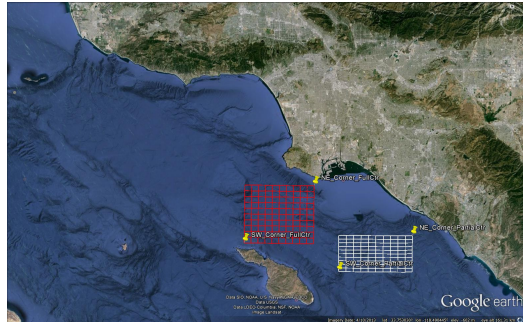
## Probabilistic completeness

**Lemma 2.** *The time-varying RRT are probabilistic complete, i.e., the expected number of iteration required to connect  $\mathbf{x}_{start}$  to  $\chi_{end}$  is limited.*

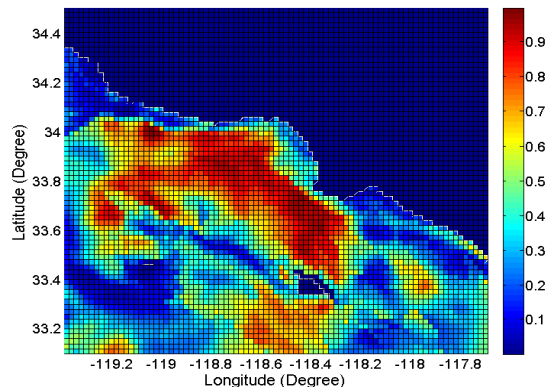
The proof for probabilistic completeness is similar to those in [24]. However, it should be noted that proofs of probabilistic completeness in previous literature deal with ideal cases of non-disturbing environments. In the scenarios of this paper, if the vehicle lies in the partial controllability areas, we cannot guarantee the attraction of sequences in  $\chi_{free}$  into  $\mathcal{B}_{\eta_f, r_f}$ .

## 8 Results

Figure 6(a) shows the the area where we will plan paths for the profilers. Figure 6(b) is the controllability map for the area in Figure 6(a). The controllability map is generated using the process depicted in Section 5. Details on generation of the controllability map can be referenced in [10]. In Figure 6(b), red indicates controllable areas, whilst blue shows less controllable areas. Moreover, land indexed in dark blue corresponds to completely uncontrollable areas.



(a) Google Earth image of the geographic region of interest



(b) The controllability heat map generated from ocean model predictions. Blue refers to areas of low controllability, and red are areas of high controllability.

Figure 6: (a) The geographic area of interest highlighted by grid rectangles. (b) The controllability heat map computed for this geographic region. Note that the two images are not the same scale.

In this work, we verify our proposed algorithms in two types of regions, including near fully-controllable and partially-controllable regions. In Figure 6(a), the fully-controllable region is represented by red grid,

Table 1: Summary of the Monte Carlo Simulations

	Convergence (%)	Avr Switchings	Avr Path Length (km)	Real Convergence (%)	Avr Difference (km)
FullCtr TI	97	44	21.983	4	8.593
FullCtr TV	100	40	22.489	100	0.405
PartialCtr TI	58	94	25.668	3	17.337
PartialCtr TV	61	48	22.012	100	0.368

whereas the partially-controllable region is illustrated with white grid. The controllability capability in those gridded regions can be easily verified by matching the regions with Figure 6(b). For instance, the white gridded region has relatively low controllability, since the region is mostly blue.

Furthermore, the gridded rectangles are chosen to have edge sizes of more than 20 km so as to present the algorithms applicable in planning long-distance missions which span several days to weeks.

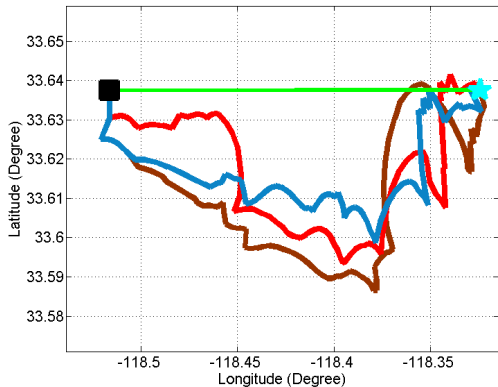


Figure 7: Planned Paths for the profiler when using time-varying algorithm

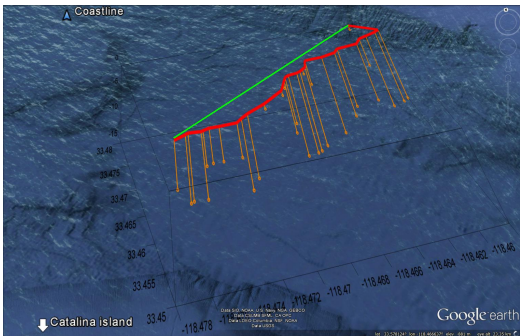


Figure 8: 3D Planned Paths when using time-varying algorithm

### 8.1 Monte-Carlo simulations of the path planner

We carry out Monte-Carlo simulations of the algorithms in both fully-controllable and partially-controllable regions of Fig. 6(a). We undertake Monte-Carlo simulation for: 1) fully-controllable time-invariant RRT, 2) fully-controllable time-varying RRT, 3) partially-controllable time-invariant RRT, and 4) partially-controllable time-varying RRT.

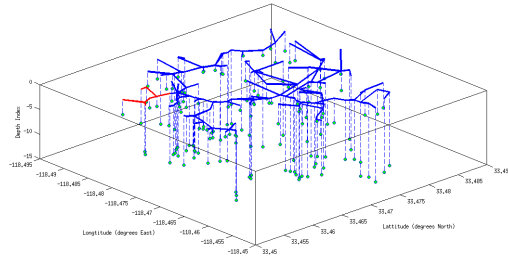


Figure 9: 3D Tree when using time-varying algorithm

For each region, 100 pairs of starting and goal waypoints are randomly generated for Monte-Carlo simulation. The algorithms in accordance with each of the aforementioned simulation cases are then executed to plan paths for every pair of the desired waypoints.

Table 1 shows a summary of the Monte-Carlo simulation for each case. Efficiency of the algorithms are assessed via five quality factors, including: 1) percentage of convergence amongst 100 runs of the algorithms, 2) an average number of depth switchings, 3) an average length of planned path, 4) percentage of real convergence, and 5) average difference (distance) between the destination goal and the planned final position. The real convergence shows the number of planned paths amongst 100 runs that actually terminate inside the ball  $\mathcal{B}_{\eta_f, r_f}$ . Here we choose  $r_f = 0.55$  km. This assessment criterion is necessary particularly to the time-invariant cases where the planned paths divert away from the destination goals once they are applied with time-varying data. Finally, the average distance criterion is the distance between the desired goal position and the actual end location of the profiler.

From Table 1, the average number of depth switchings is greater than or equal to 40. Hence, time required to complete a planned path is nearly two days on average given the vehicle’s depth changing rate is 1 switching/hour. The average travel distance and time suggest algorithms be suitable to motion planning for persistent navigation.

The average switchings of the full controllability cases are less than those of the partial controllability ones. This phenomenon can be explained by the fact that the profilers operating in the partial-controllable region do not have a variety of choices of control actions, and thus tend to take longer paths which are sometimes away from the goal.

If the controllability check indicates the region is only partially controllable, both time-invariant and time-varying algorithms return less than 100% convergence. This is due to the fact that ocean currents in the region are dominating in only some directions.



As we discuss in the Analysis section, vectors of the ocean currents in the region do not span the space, leads to uncontrollable states of the system.

Nevertheless, whenever the time-varying path planner return a path, it can guarantee that the path's real end position falls within the terminating ball  $\mathcal{B}_{\bar{\eta}_f, r_f}$  since the real convergence of such algorithm is 100%.

In addition, the time-varying RRT is capable of searching more convergence paths than those of time-invariant even though both of the path planners operates in partially-controllable areas. In fact, the condition of time-independent currents in the time-invariant RRT restricts the number of variations of ocean currents' directions. Thus, it decreases the number of current vectors spanning the space. Consequently, it is less likely that the time-invariant RRT can find a converged path as compared to the time-varying one.

A notable number emerging from the summary is that we can make the profiler converge to the goal almost surely (100%) when the time-varying RRT is applied inside the fully-controllable region. It is also almost surely to assure the real convergence of time-varying algorithm operating inside the fully-controllable region. Even though the time-invariant algorithm shows 97 out of 100 simulations converge, only 4% of the planned paths terminating within  $\mathcal{B}_{\bar{\eta}_f, r_f}$ . This fact is construed by observing that the average distance between the real end locations and the goal destinations for the fully-controllable time-invariant algorithm is slightly more than 8.5 km and much greater than  $r_f$ .

In summary, the time-varying RRT with prior controllability check formulate a combined algorithm that can guarantee convergence of the profiling floats. Also, the time-varying RRT is obviously superior than the time-invariant one when they are applied to plan paths in 4D space.

## 8.2 Time-varying planned paths and trees

Figure 7 shows various planned paths returned from the time-varying RRT. The green line is a connecting line between the starting waypoint and the destination goal. Distance between waypoints in Figure 7 is more than 10 km. Lines in red, blue, and brown are planned trajectories returned from different executions of the algorithms. Due to randomness of the RRT, we have different paths after each run. However, all of the paths converge to the area around the goal destination.

Figure 8 shows the expected trajectory when executing one of the planned paths of Figure 8. Similarly, the green line is the connecting line of desired waypoints. The trajectory include sections in horizontal planes represented in red, and sections of depths changing represented in orange. This figure illustrate the fact that the profiler changes its depths, picking appropriate currents to navigate towards the goal.

Figure 9 presents a RRT tree generated from the time-varying algorithm. This tree shows the evolution of the profiling float locations at different points of time. Particularly, in this figure, red and blue subtrees represents the time-dependent evolution of the tree

from the root node. Since the tree evolution accounts for longitudinal, latitudinal, depths, and time, this tree is actually of 4 dimensions

## 9 Conclusion

In this paper, we presented a set of algorithms that plan paths for profiling floats based on predictions from an OMP that guarantee arrival to the goal. We incorporate high levels of uncertainty of a dynamic ocean, while still maintaining convergence properties along the path.

Several Monte-Carlo simulations demonstrate the effectiveness of the method, and show 100% of paths converge compared with less than 5% that converge when not considering the time-varying dynamics of the ocean.

## Acknowledgments

V. Huynh was supported by QUTPRA scholarship from the Queensland University of Technology. R.N. Smith was supported through a Fort Lewis College Deans award for innovative research. This work relates to Department of the Navy Grant N62909-11-1-4046 issued by the Ofce of Naval Research Global. The United States Government has a royalty-free license throughout the world in all copyrightable material contained herein.

## References

- [1] O. Schofield, J. Kohut, D. Aragon, E.L. Creed, J.G. Graver, C. Haldman, J. Kerfoot, H. Roarty, C. Jones, D.C. Webb, and S. Glenn. Slocum gliders: Robust and ready. *Journal of Field Robotics*, 24(6):473–485, 2007.
- [2] Gwynn Griffiths, Clayton Jones, James Ferguson, and Neil Bose. Undersea gliders. *Journal of Ocean Technology*, 2(2):64–75, 2007.
- [3] Dean Roemmich, Stephen Riser, Russ Davis, and Yves Desaubies. Autonomous profiling floats: Workhorse for broad-scale ocean observations. *Marine Technology Society Journal*, 38:21–29, 2004.
- [4] Joshua Grady Graver. *Underwater Gliders: Dynamics, Control and Design*. PhD thesis, Princeton University, 2005.
- [5] D.A. Paley, F. Zhang, and N.E. Leonard. Cooperative control for ocean sampling: The glider coordinated control system. *IEEE Transactions on Control Systems Technology*, 16(4):735–744, July 2008.
- [6] Naomi E. Leonard, Derek A. Paley, Russ E. Davis, David M. Fratantoni, Francois Lekien, and Fumin Zhang. Coordinated control of an underwater glider fleet in an adaptive ocean sampling field experiment in monterey bay. *Journal of Field Robotics*, 27(6):718–740, 2010. ISSN 1556-4967.
- [7] Ryan N. Smith, Yi Chao, Peggy P. Li, David A. Caron, Burton H. Jones, and Gaurav S. Sukhatme. Planning and implementing trajectories for autonomous underwater vehicles to track

- evolving ocean processes based on predictions from a regional ocean model. *International Journal of Robotics Research*, 29(12):1475–1497, October 2010.
- [8] Ryan N. Smith, Mac Schwager, Stephen L. Smith, Burton H. Jones, Daniela Rus, and Gaurav S. Sukhatme. Persistent ocean monitoring with underwater gliders: Adapting sampling resolution. *Journal of Field Robotics*, 28(5):714 – 741, September/October 2011.
- [9] Jerome Jouffroy, Qiuyang Zhou, and Oliver Zielinski. On active current selection for lagrangian profilers. *Modeling, Identification and Control*, 2013.
- [10] Ryan N. Smith and Van T. Huynh. Controlling buoyancy-driven profiling floats for applications in ocean observation. *IEEE Journal of Oceanic Engineering*, 2014.
- [11] Chris Roman, Gabrielle Inglis, and Bryan McGilvray. Lagrangian floats as sea floor imaging platforms. *Continental Shelf Research*, 31(15): 1592 – 1598, 2011. ISSN 0278-4343.
- [12] David Hsu, Robert Kindel, Jean-Claude Latombe, and Stephen Rock. Randomized kinodynamic motion planning with moving obstacles. *The International Journal of Robotics Research*, 21(3):233–255, 2002.
- [13] Weizhong Zhang, T. Inanc, S. Ober-Blobaum, and J.E. Marsden. Optimal trajectory generation for a glider in time-varying 2d ocean flows b-spline model. In *Robotics and Automation, 2008. ICRA 2008. IEEE International Conference on*, pages 1083–1088, May 2008.
- [14] N.K. Yilmaz, C. Evangelinos, P. Lermusiaux, and N.M. Patrikalakis. Path planning of autonomous underwater vehicles for adaptive sampling using mixed integer linear programming. *Oceanic Engineering, IEEE Journal of*, 33(4):522 – 537, oct. 2008. ISSN 0364-9059.
- [15] K.P. Carroll, S.R. McClaran, E.L. Nelson, D.M. Barnett, D.K. Friesen, and G.N. William. Auv path planning: an a\* approach to path planning with consideration of variable vehicle speeds and multiple, overlapping, time-dependent exclusion zones. In *Autonomous Underwater Vehicle Technology, 1992. AUV '92., Proceedings of the 1992 Symposium on*, pages 79–84, Jun 1992.
- [16] Alberto Alvarez and Andrea Caiti. Interaction of autonomous underwater vehicles with variable scale ocean currents. In *Proceedings of the IFAC World Conference Systems*, 2002.
- [17] Alberto Alvarez, Andrea Caiti, and Reiner Onken. Evolutionary path planning for autonomous underwater vehicles in a variable ocean. *IEEE Journal of Oceanic Engineering*, 29(2):418–429, 2004.
- [18] B. Garau, A. Alvarez, and G. Oliver. Path planning of autonomous underwater vehicles in current fields with complex spatial variability: an a\* approach. In *Robotics and Automation, 2005. ICRA 2005. Proceedings of the 2005 IEEE International Conference on*, pages 194 – 198, april 2005.
- [19] B. Garau, M. Bonet, A. Alvarez, S. Ruiz, and A. Pascual. Path planning for autonomous underwater vehicles in realistic oceanic current fields: Application to glider in the western mediterranean sea. *Maritime Research*, 6:5–22, 2009.
- [20] Dov Kruger, Rustam Stolkin, Aaron Blum, and Joseph Briganti. Optimal auv path planning for extended missions in complex, fast-flowing estuarine environments. In *Proceedings of the IEEE International Conference on Robotics and Automation*, Rome, Italy, 2007.
- [21] Jonas Witt and Matthew Dunbabin. Go with the flow: Optimal path planning in coastal environments. In J. Kim and R. Mahony, editors, *Proceedings of the 2008 Australasian Conference on Robotics & Automation (ACRA 2008)*, Canberra, ACT, 2008. ISBN: 9780646506432.
- [22] L.E. Kavraki, P. Svestka, J.-C. Latombe, and M.H. Overmars. Probabilistic roadmaps for path planning in high-dimensional configuration spaces. *Robotics and Automation, IEEE Transactions on*, 12(4):566–580, Aug 1996. ISSN 1042-296X.
- [23] Steven M. LaValle and James J. Kuffner. Randomized kinodynamic planning. *The International Journal of Robotics Research*, 20(5):378–400, 2001.
- [24] Sertac Karaman and Emilio Frazzoli. Sampling-based algorithms for optimal motion planning. *The International Journal of Robotics Research*, 30(7):846–894, 2011.
- [25] A. Bry and N. Roy. Rapidly-exploring random belief trees for motion planning under uncertainty. In *Robotics and Automation (ICRA), 2011 IEEE International Conference on*, pages 723–730, May 2011.
- [26] Dushyant Rao and Stefan B. Williams. Large-scale path planning for underwater gliders in ocean currents. In *Australian Conference on Robotics and Automation (ACRA)*, 2009.
- [27] A.F. Shchepetkin and J.C. McWilliams. Quasi-monotone advection schemes based on explicit locally adaptive dissipation. *Monthly Weather Review*, 126:1541–1580, 1998.
- [28] Alexander F. Shchepetkin and James C. McWilliams. The regional oceanic modeling system (ROMS): a split-explicit, free-surface, topography-following-coordinate oceanic model. *Ocean Modelling*, 9:347–404, 2005.